Influence of cluster morphology on calculation of the aggregation rate constant in mesoscopic systems

A. Fernández-Barbero,[1,*] A. Schmitt,[2] M. A. Cabrerizo-Vílchez,[2] R. Martínez-García,[2] and R. Hidalgo-Álvarez[2]

[1]*Grupo de Física de Fluidos Complejos, Departamento de Física Aplicada, Universidad de Almería, Cañada de San Urbano s/n, E-04120 Almería, Spain*

[2]*Grupo de Física de Fluidos y Biocoloides, Departamento de Física Aplicada, Universidad de Granada, E-18071 Granada, Spain*

(Received 31 December 1996)

The aggregation of monodisperse polystyrene microspheres is studied in processes induced at high salt concentration. Measurements were taken using single-cluster light scattering (free model technique) and photon correlation spectroscopy. Two cluster growth models were used to study the effect of the cluster morphology on the calculation of the rate constant. The rate constants were measured as a function of the particle concentration in order to control the aggregation time scale. At high particle concentration, rate constant deviations from the theoretical one was observed, which was explained by taking into account the fractal structure of the clusters for early aggregation stages. [S1063-651X(97)08409-2]

PACS number(s): 82.70.Dd, 64.60.Cn, 05.40.+j

I. INTRODUCTION

Over the past few years, considerable interest has been focused on the study of dynamic structures, in which an irreversible addition of primary particles leads to cluster formation. The aggregation in mesoscopic systems that consist of an aqueous solution of nanoparticles (a colloidal solution) is a good model for describing this phenomenon, central to many physical [1], chemical [2], and biological [3] processes. Two universal regimes, independent of the particle nature, have been found for colloidal aggregation: diffusion-limited cluster aggregation (DLCA) and reaction-limited cluster aggregation (RLCA) [4–10]. For DLCA the probability that collisions between particles give rise to cluster formation is equal to one and for RLCA it is lower. This probability depends on the interaction between the clusters, which may be controlled by adding salt to a stable colloid. The time evolution of the cluster-size distribution is usually described by Smoluchowski's coagulation equation [11] and the fractal structure of the aggregates is characterized by a fractal dimension d_f [12,13].

Single-cluster light scattering (SCLS) offers perhaps the most unambiguous methods for monitoring aggregation. This technique allows detailed cluster-size distributions to be measured at different aggregation stages by directly counting clusters throughout the processes [14–21]. The aggregation rate may be determined from the time evolution of the cluster-size distribution by using the Smoluchowski coagulation equation. Nevertheless, the forces involved in cluster separation can break up the aggregates under extreme experimental conditions. As an alternative technique, photon correlation spectroscopy (PCS) is frequently employed for studying aggregating systems [22]. Its advantage is that the systems are not altered during measurements. However, theoretical models must be used to fit the measured autocorrelation functions. Guinnup and Schultz [23], for example, researched the aggregation of polystyrene lattices by deconvoluting the intensity autocorrelation function using an iterative procedure. Herrington and Midmere [24] applied a simpler method that avoided the tedious deconvolution process. They assumed the Smoluchowski kinetics for early stages of aggregation and the Rayleigh-Gans-Debye (RGD) approximation for the scattered intensity [25]. Moreover, a cluster growth model must be assumed in order to determine the RGD form factor and the diffusion coefficient for each j-fold cluster. So a theoretical autocorrelation function is generated and fitted to the experimental ones by varying the degree of aggregation. In this paper the aggregation kinetics of monodisperse polystyrene microspheres is studied in processes induced at high salt concentration. Measurements are taken using two techniques: SCLS and PCS, offering the possibility of covering a wider range of particle concentration and comparing results obtained by two such different techniques. Furthermore, we modify the Herrington-Midmere method by incorporating two alternative cluster growth models, which generate aggregates with different morphology and so the influence of cluster morphology in the calculation of the rate constant is studied.

The rate constants are measured at different particle concentrations, which allows the aggregation time scale to be scaled. The data are compared with the value obtained from the theoretical model including viscous effect. At high particle concentration, a rate constant deviation from the theoretical value is observed, which is explained by taking into account the fractal structure of the clusters for early aggregation stages. This explanation is corroborated by measurements of the fractal dimension.

This paper is structured as follows. Section II includes a theoretical background. Section III describes materials and methods. The latter involve a description of the SCLS instrument, the PCS method employed to measure rate constants, the experimental system, the particle characterization, and experimental details. Section IV gives the results and a discussion thereof. Section V covers the conclusions.

*Author to whom correspondence should be addressed. Electronic address: AFERNAND@UALM.ES

II. THEORY

A. Aggregation kinetics

The Smoluchowski equation [11]

$$\frac{dN_n}{dt}=\frac{1}{2}\sum_{i+j=n}k_{ij}N_iN_j-N_n\sum_{i=1}^{\infty}k_{in}N_i \tag{1}$$

describes the temporal evolution of the cluster-size distribution $N_n(t)$ for diluted solutions. The physical information is contained in the kernels k_{ij}, which parametrize the rate at which i-mers bond to j-mers. The first term in this equation represents the mean rate at which n-mers are formed by the aggregation of i-mers and j-mers. The second term represents the rate at which n-mers disappear when they aggregate with any i-mers to form $(n+i)$-mers. Analytical solutions for the coagulation equation may be obtained only for simple mathematical forms of the kernels.

Considering a constant kernel, i.e., $k_{ij}=k_{11}$, and initial monomeric conditions $N_n(t=0)=N_0\delta_{1n}$, the solution is given by [26]

$$N_n(t)=N_0\frac{\left(\frac{t}{t_{\mathrm{agg}}}\right)^{n-1}}{\left(1+\frac{t}{t_{\mathrm{agg}}}\right)^{n+1}}, \tag{2}$$

where N_0 is the initial monomer concentration and $t_{\mathrm{agg}}\equiv 1/N_0k_s$ is the aggregation time scale. For a system of spherical particles moving in a medium of viscosity η, the rate constant k_s is given by [11]

$$k_s^{\mathrm{Brow}}=\frac{4}{3}\frac{k_BT}{\eta}. \tag{3}$$

B. Viscous interaction

The stability of colloidal solutions is determined by the interactions between each pair of particles. The interparticle potential is usually described by the Derjaguin-Landau-Verwey-Overbeek theory [27,28]. This includes London–van der Waals attraction forces and electrostatic repulsion due to the charge on the surface of spherical particles. The stability factor W is defined as the ratio of the aggregation rates for noninteracting particles (DLCA) and for particles with a finite interaction (RLCA). W is a measure of the stability of colloidal dispersions. In RLCA, only a fraction $1/W$ of the collisions leads to the formation of a bond. In diluted colloids, the particle encounters are treated as binary collisions and their frequency is obtained by solving the diffusion equation. Fuchs [29,30] derived the following relationship between the total potential energy $V_T(h)$ and the stability factor

$$W=2\int_2^{\infty}\frac{\exp\left(\frac{V_T(h)}{k_BT}\right)}{h^2}\,dh, \tag{4}$$

where $h=(H+2a)/a$ for two spherical particles of equal radii a, H is the minimum distance between two spheres, k_B is the Boltzmann constant, and T is the temperature. The total potential energy $V_T(h)$ is defined as V_r+V_a, where V_r and V_a are the repulsive and attractive potential energies, respectively. The expression used in this paper for the repulsive energy was proposed by Ohshima and Kondo [31]. For the attraction potential energy we employed the classical formula appearing in Ref. [28].

The modified stability factor W_{visc} has to be calculated in order to assess the influence of viscous interaction. According to Spielman [32], W_{visc} may be written as

$$W_{\mathrm{visc}}=2\int_2^{\infty}\left(\frac{D_{12}^{\infty}}{D_{12}}\right)\exp\left(\frac{V_T(h)}{k_BT}\right)\frac{dh}{h^2}, \tag{5}$$

where $D_{12}=k_BT/f$ is the Brownian diffusivity for relative motion, f is the hydrodynamic resistance coefficient, and D_{12}^{∞} is the relative diffusivity at infinite separation. D_{12} depends on viscosity, particle dimensions, and the relative separation between particles. A numerical assessment of D_{12} has been performed in this paper using formulas from Spielman's article. D_{12} undergoes a large drop when the particle separation is smaller than the particle radius. Viscous interaction modifies the value of the rate constant (3), which may now be calculated by [33]

$$k_s^{\mathrm{vis}}=\frac{4}{3}\frac{k_BT}{\eta}\frac{1}{W_{\mathrm{vis}}}. \tag{6}$$

III. MATERIAL AND METHODS

A. Single-particle light scattering

Single-particle optical detection is one of the most advanced techniques for measuring particle-size distributions and monitoring aggregation processes. We briefly present a single-particle optical sizer built in our laboratory [34–36] based on the device of Pelssers, Stuart, and Fleer [14,15]. In this technique, single clusters, insulated by hydrodynamic focusing of a colloidal dispersion, are forced to flow across a focused laser beam. A measurement of the cluster-size distribution is taken by analyzing the light intensity scattered by single clusters at low angle, where intensity is monotonically related to the square cluster volume: $I_n(\theta)/I_1(\theta)=n^2\sim V^2$. Under this condition, the scattered light intensity is high enough to detect particles accurately and the strong sensibility of the scattered light intensity on the particle volume makes it possible for a high resolution to be achieved. For larger angles the intensity is lower and data interpretation becomes difficult due to intensity oscillations appearing when the particle size changes [25].

Figure 1 shows a block diagram of the instrument. Basically, it is a flow ultramicroscope in which pulses of light from single particles are detected. Light from a laser is sent through an input optical system in order to create a homogeneously illuminated zone at the center of the flow cell, where cluster separation is performed. In the focusing cell, a colloidal dispersion is injected into a fast flowing water stream, thereby obtaining a narrow particle stream. Single particles cross this illuminated zone, scattering pulses of light. Detection optics selects only the light scattered at low angle and focuses it onto a photomultiplier, which supplies a propor-

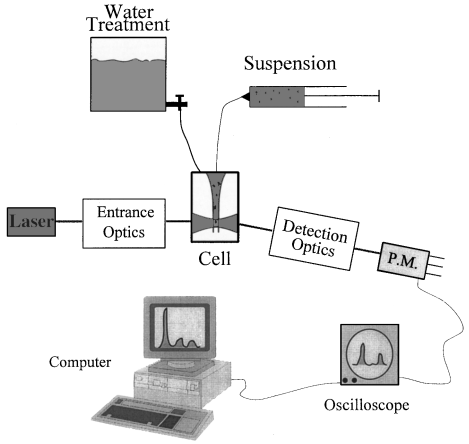

FIG. 1. Block diagram of the experimental setup. P.M. denotes photomultiplier.

tional electrical current. This signal is converted into voltage and digitalized. A computer controls the analog to digital converter board and recognizes, classifies, and counts the pulses by running an algorithm on-line.

A simpler way to determine the rate constant k_{11} is to use Smoluchowski's equation for the evolution of the number of primary particles. Performing a simple algebraic transformation from Eq. (2), one obtains for the inverse square root of the monomer concentration N_1 the following linear function of time

$$\frac{1}{\sqrt{N_1(t)}} = \frac{1}{\sqrt{N_0}}\,(1+N_0 k_s t). \tag{7}$$

Thus the plot $N_1^{-1/2}$ vs t should give a straight line when the constant kernel describes the aggregation process. It is then possible to obtain the initial monomer concentration N_0 and the rate constant k_s from the intersection and the slope, respectively.

B. Photon correlation spectroscopy

Photon correlation spectroscopy relies on the fluctuation in the light scattered from disperse particles undergoing Brownian motion. The autocorrelation function $G(\tau)$ is calculated from the product of two photon counts at time t and time $t+\tau$ such that $G(\tau)=\langle I(t)I(t+\tau)\rangle$. The normalized intensity autocorrelation function $g^{\text{int}}(\tau)$ is given by [22]

$$g^{\text{int}}(\tau) = \frac{\langle I(t)I(t+\tau)\rangle}{\langle I(t)I(t)\rangle}. \tag{8}$$

The function $g^{\text{int}}(\tau)$ is related to the normalized field autocorrelation function $g^{\text{field}}(\tau)$ by the Siegert relationship [22]

$$g^{\text{field}}(\tau) = 1 + C|g^{\text{int}}(\tau)|^2, \tag{9}$$

where C is a constant determined by the optics of the instrument. The field autocorrelation function for a suspension of clusters made up from monodisperse spheres is given by [37]

$$g^{\text{field}}(\tau) = \sum_{j=1}^{j_{\max}} G_j \exp(-\Gamma_j \tau), \tag{10}$$

where

$$G_j = \frac{N_j\langle i_j(\theta)\rangle}{\Sigma_{j=1}^{j_{\max}} N_j\langle i_j(\theta)\rangle}, \quad \Gamma_j = q^2 D_j\,. \tag{11}$$

In the formula above, q is the scattering wave vector [$q=4\pi/\lambda\,\sin(\theta/2)$, where λ is the wavelength of the light in the solvent and θ is the scattering angle]. N_j is the cluster-size distribution (particle number density of each j-fold cluster), D_j is the diffusion coefficient of the j-fold cluster, and $i_j(\theta)$ is the intensity scattered by a single j-fold cluster.

The scattered intensity is given by [38]

$$i_j(\theta) = i_1(\theta) P_j(\theta), \tag{12}$$

where $i_1(\theta)$ is the intensity scattered for a monomer and $P_j(\theta)$ is the form factor for a j-fold cluster that is given by the RGD approximation

$$P_j(\theta) = j + 2\sum_{n,m}^{j} \frac{\sin(q r_{nm})}{q r_{nm}}. \tag{13}$$

In this equation r_{nm} is the separation between the centers of the spheres n and m and the sum is extended to all pairs of monomers in the cluster. Combining all this information, the field autocorrelation function has the form

$$g^{\text{field}}(\tau) = \frac{\sum_{j=1}^{j_{\max}} N_j(t/t_{\text{agg}})\langle P_j(\theta)\rangle \exp(-\Gamma_j\tau)}{\sum_{j=1}^{j_{\max}} N_j(t/t_{\text{agg}})\langle P_j(\theta)\rangle}. \tag{14}$$

In order to find $\langle P_j(\theta)\rangle$, random clusters were generated by a computer program, following work reported in Refs. [24] and [39]. Moreover, the radius of gyration of each generated cluster R_g was determined and identified to the hydrodynamic radius (only for small clusters). Thus the diffusion coefficient D_j was obtained by using the Einstein-Stokes formula and Γ_j was estimated.

A change has been introduced in the cluster simulation with respect to that of Herrington and Midmore [24] in order to study the effect of the cluster morphology on the calculation of the rate constant. The simulations were performed following two different criteria. In the former, an $(n+1)$-mer is obtained by shooting a monomer into the center of mass of an n-mer. In the second algorithm, an $(n+1)$-mer grows by shooting a monomer in random directions. So it is expected that the first model generate more compact clusters than the second one. The first algorithm will be called the compact-cluster model and the second one the branched-cluster model. Figure 2 shows the average radius of gyration as a function of the cluster size using the two growth algorithms. Monomers were 150 nm in radius and the simulations were performed up to $n=50$, which is the maximum cluster size used in our study (early steps of the aggregation). The results show an evident effect of compactness. The branched clusters are bigger than the compact

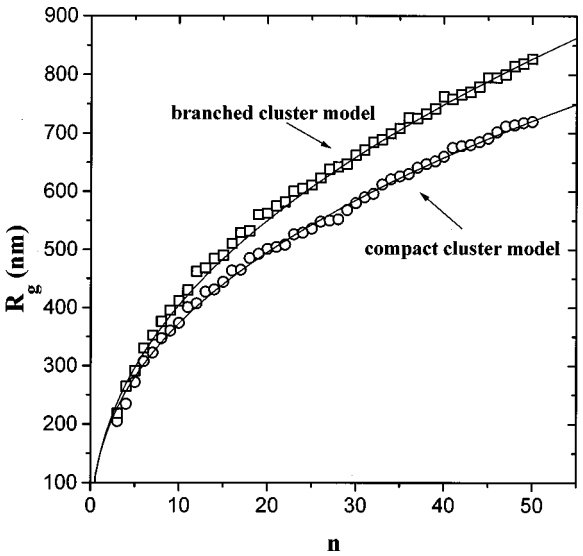

FIG. 2. Average radius of gyration as a function of the cluster size using the compact-cluster model (○) and the branched-cluster model (□).

clusters and when the cluster size increases, the difference in the radius of gyration increases. In order to characterize cluster compactness, the fractal dimension of the clusters was determined by using the relationship [40]

$$R_g(n) = R_0 n^{1/d_f}, \tag{15}$$

where R_0 is the monomer radius. For the compact-cluster model a fractal dimension 2.44 ± 0.03 was found and using the branched-cluster model it was 2.25 ± 0.02.

Our aim is to measure the rate constants by monitoring the processes during the early aggregation stages. Following Herrington and Midmore [24], we fitted the theoretical field autocorrelation function (14) to the experimental one, with the fitting parameter being the scaled time $T = t/t_{\text{agg}}$. For each time t, we had a normalized time T and by plotting T vs t, the aggregation time scale $t_{\text{agg}} \equiv 1/N_0 k_s$ was measured. The rate constants k_s were calculated from t_{agg} once the initial monomer concentration N_0 was known. The photon correlation instrument used to measure the intensity autocorrelation function was a Malvern 4700 (United Kingdom) with a He-Ne TEM_{00} laser working at a wavelength of 632.8 nm.

C. Experimental system and details

The experimental systems were two monodisperse polystyrene lattices. Table I shows the principal characteristics. The lattices had a negative surface charge due to sulphate groups. The lattices were cleaned by centrifugation or serum replacement, followed by ion exchange over a mixed bed. The size of the microspheres was determined by transmission electron microscopy. The critical coagulation concentration (CCC) was estimated directly by dilution of latex particles in solutions of different KCl concentration. All chemicals used were of high quality and twice-distilled water was purified using Millipore equipment.

Prior to undertaking our studies, fresh suspensions of microspheres were sonicated for 30 min to break up any initial clusters. Aggregation was initiated by mixing the microspheres suspended in salt-free water and the aggregation agent. Aggregations were induced at high ionic concentration: $0.5M$ of KCl, higher than the CCC. Immediately afterward, the timer was started.

The temperature was controlled by an external thermostat. Both the latex and the electrolyte were kept at the desired temperature for 30 min prior to measuring. The cluster sedimentation due to the slight difference between polystyrene and water densities was negligible.

The aggregation experiments monitored by SCLS were carried out in a reaction vessel. Precautions were taken so that nondestructive size distribution analysis could be performed. Small portions of aggregating colloid were slowly taken from the suspensions through a wide aperture pipette. Samples were diluted in the same solvent used for the dispersions in order to stop aggregation during the measurements. No variations in the cluster-size distribution were detected while the samples were kept in the dilute medium for several hours. Moreover, the particle concentration was optimized to ensure single-particle detection ($\approx 10^7$ cm^{-3}). Cluster-size distribution was monitored and histograms were taken at different aggregation steps. These measurements allowed the cluster-size distribution to be determined.

The PCS measurements were carried out in a 0.5-cm cylindrical cuvette. The scattering angle was 60°. The time of measurement for each autocorrelation function was 45 s, short enough to guarantee that the samples were at the same aggregation stage during the measurement.

IV. RESULTS AND DISCUSSION

A. Measuring rate constants

The rate constants k_s were determined using two alternative techniques: SCLS and PCS. In previous papers [35,36] we demonstrated that the constant kernel describes the time evolution of the cluster-size distribution for aggregation times shorter than $7.2 t_{\text{agg}}$. Therefore, the constant kernel solution of the Smoluchowski equations was chosen to fit the experimental data for short aggregation times.

Using the single-particle light-scattering instrument, the rate constants k_s were obtained by plotting the inverse square root of the monomer concentration as a function of time. Figure 3 shows experimental curves for sample AS8. According to Eq. (7), straight lines were obtained, which confirms once again that the constant kernel is suitable. The rate

TABLE I. Summary of the systems employed.

Sample	Source	Surface	Cleaning	Radius (nm)	CCC (M)	Technique employed
RP-300	Rhône-Poulenc	sulphate	centrifugation and ion exchange	150 ± 11	≈ 0.11	PCS
AS8	Universidad de Granada	sulphate	serum replacement and ion exchange	290 ± 14	≈ 0.10	SCLS

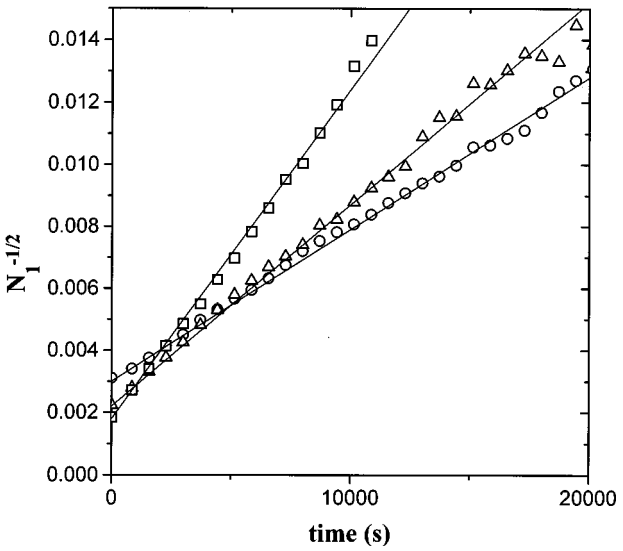

FIG. 3. Inverse square root of the monomer concentration as a function of time measured by SCLS for three different particle concentrations. The rate constants were calculated from the slope.

constants k_s were calculated from the slope.

The experimental data obtained by PCS were assessed using the two different algorithms described in Sec. III. The normalized time T was plotted as a function of the time t assuming the compact-cluster model or branched-cluster model, respectively. Figure 4 shows typical results for the compact growth model. The straight lines are in good agreement with the theoretical prediction for the constant kernel. k_s was calculated from the slope $N_0 k_s$ once the initial particle concentration N_0 was known.

B. Dependence of k_s on the initial particle concentration N_0

In this section the influence of the initial particle number density N_0 on the Smoluchowski rate constants k_s was studied using PCS and single-particle light scattering. Figure 5 plots k_s as a function of N_0 for fast aggregation (0.5M KCl). At low N_0, the aggregation rates tend to be constant. Moreover, the values obtained by PCS using the compact-cluster model coincide perfectly with the values measured by the single-particle instrument (free model technique). At higher initial particle concentrations the rate constants increase monotonically. The rate constants k_s calculated with the branched-cluster model are significantly smaller than the ones obtained with the compact model.

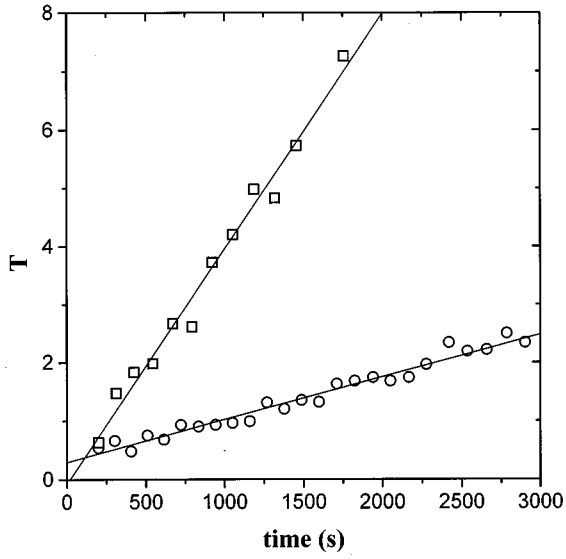

FIG. 4. Normalized time T ($=t/t_{agg}$) as a function of the time t for two different particle concentrations: $N_0=3.0\times10^8$ cm^{-3} (○) and $N_0=1.2\times10^9$ cm^{-3} (□). The compact growth model was employed. The rate constant may be calculated from the slope $N_0 k_s$ once the initial particle concentration N_0 is known.

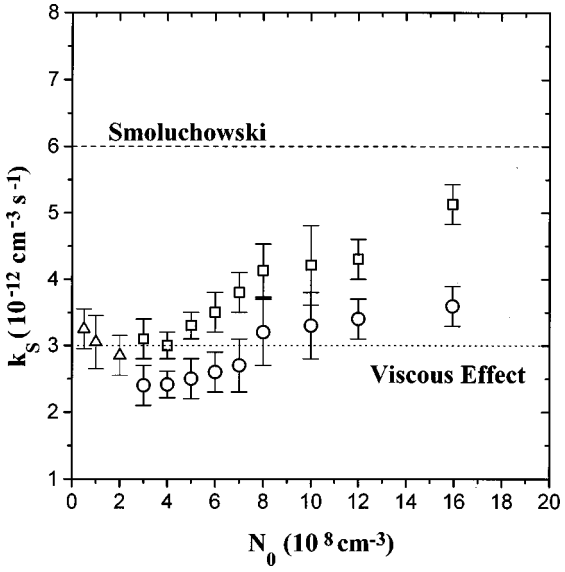

FIG. 5. Rate constant as a function of the initial particle concentration for fast aggregation measured by SCLS (△), PCS (□) (compact-cluster model), and PCS (○) (branched-cluster model). Dashed lines are the theoretical Smoluchoski value and the rate constant corrected by viscous interaction.

At low N_0, the rate constants measured with PCS (compact-cluster model) and SCLS coincide and fall within the range of values commonly reported for fast aggregation [15,36,41–52]. For our experimental conditions, the theoretical Smoluchowski rate constant is 6.0×10^{-12} cm^{-3} s^{-1}, which is about twice the experimental value. In order to explain the difference, viscous interaction between the particles was considered. The modified stability factor W_{vis} was numerically assessed using Eq. (5) and Spielman's formulas [32]. From these calculations $W_{vis}=1.97$ was found and, using Eq. (6), $k_s^{vis}=3.0\times10^{-12}$ cm^{-3} s^{-1}, which coincides perfectly with the experimental value obtained by SCLS and PCS with the compact-cluster model. This confirms the idea that clusters grow very compactly during the early stages of aggregation and shows that their branched structure is still not relevant.

At higher initial particle densities, the rate constants k_s deviate from the theoretical value and increase with increasing N_0. This behavior is somewhat unexpected since, according to Eq. (6), it should be N_0 independent. Deviations from Smoluchowski kinetics for fast aggregation were found for gold sols [53] and polystyrene latex [38,41,54,55]. Nevertheless, other authors [48,49,52] inferred rate constants that were independent of the initial number density. So this discrepance is not still explained, which makes this matter interesting. Lips and Willis proposed that these discrepancies

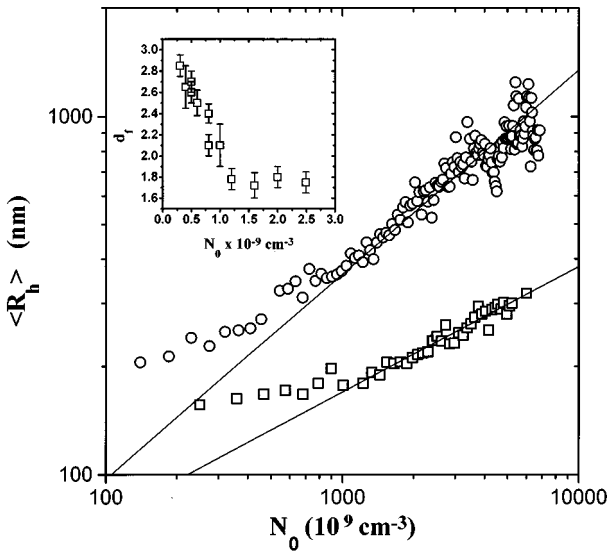

FIG. 6. Time evolution of the hydrodynamic radius. The fractal dimension is calculated from the asymptotic behavior at long times for two different particle concentrations: $N_0 = 2.5\times10^9$ cm^{-3} (○) and $N_0 = 3.0\times10^8$ cm^{-3} (□). The fractal dimension as a function of N_0 is plotted in the left-hand upper corner. At low number density, the fractal dimension tends towards 3, the dimension of space. As N_0 increases, the fractal dimension decreases and reaches the value 1.8.

were due to the erroneous assumption of the constant kernel approximation. Therefore, only average rate constants are measured, which moreover, may be technique dependent. We are going to propose another interpretation.

From our data we observed that at low N_0 the compact-cluster model leads to k_s close to the theoretical value. For N_0 of the order of 1.0×10^9 cm^{-3}, the branched-model offers better results and finally, for higher N_0, both models give values higher than the prediction. We interpret this behavior by taking into account that for low N_0 the kinetics is so slow that only small clusters appear with a fractal structure not yet established. Thus the compact model, which gives rise to clusters with a fractal dimension of 2.44 ± 0.03, works better. As N_0 increases, the aggregation process becomes faster so that bigger clusters grow. In this case, the fractal structure of the aggregates starts to be relevant and the branched model with a fractal dimension of 2.25 ± 0.02 reproduces the theoretical value. For even bigger number densities, neither model offers good results since the expected fractal dimension is of the order of 1.8 [7].

PCS was used for measuring the fractal dimension as a function of N_0 in order to support our conclusions. Figure 6 shows the time evolution of the hydrodynamic radius applying cummulant analysis [56,57]. From the asymptotic behavior at long times the fractal dimension was determined by the aid of the relationship [58]

$$\langle R_h \rangle \sim t^{1/d_f(1-\lambda)}, \tag{16}$$

where d_f is the fractal dimension and λ is the homogeneity parameter [59].

For diffusion-limited aggregation the homogeneity parameter λ, which characterizes the aggregation mechanism, has the value 0 [7,8,35,36]. Figure 6 also plots the fractal dimensions as a function of N_0 (upper left-hand corner). It may be seen that at low number density, the fractal dimension tends towards 3, the dimension of space. As N_0 increases, the fractal dimension decreases and reaches the value ≈1.8, generally accepted for fast aggregation. It should be pointed out that for $N_0 = 5.0\times10^8$ cm^{-3}, d_f gives a value of about 2.5, close to the fractal dimension obtained by the compact model (2.44). At $N_0 = 1.0\times10^9$ cm^{-3}, d_f is of the order of 2.1, which is close to the fractal dimension of the branched model (2.25). This means that the measured fractal dimensions coincide with those obtained by the different growth models within the N_0 ranges for which these models work satisfactorily. At higher initial particle concentrations, both ballistic models fail and therefore a new model that accounts for cluster-cluster aggregation should be developed. Models of this type yield more branched clusters having a fractal dimension of the order of 1.8.

V. CONCLUSION

The aggregation kinetics of monodisperse polystyrene microspheres was studied in processes induced at high salt concentration. Smoluchowki's rate constants were determined using two alternative techniques: SCLS and PCS. The rate constants were obtained from the time evolution of monomers using the single-particle instrument and by monitoring the evolution of the intensity autocorrelation function by PCS. The experimental data obtained by PCS were assessed using two different algorithms (compact-cluster model and branched-cluster model) that account for the cluster morphology in the calculation of the rate constant.

The influence of the initial particle concentration on Smoluchowski's rate constants was studied. At low N_0, the aggregation process was found to be diffusion controlled. The rate constants obtained by PCS using the compact-cluster model coincided with the values measured by SCLS (the more direct technique). This confirms the idea that clusters grow very compactly during the early aggregation stages. At higher initial particle concentration, the rate constants coincided with the theoretical value only when the branched-cluster model was used. The aggregation process speeds up so that bigger clusters grow and the fractal structure of the aggregates starts to develop. For even higher particle concentration, neither of these ballistic models offered good results. At this stage of aggregation, the aggregates show a fully developed fractal structure and therefore a more realistic model that accounts for cluster-cluster aggregation should be employed. The fractal dimensions were measured by PCS as a function of N_0 in order to support our explanation. These coincide with those obtained by the different growth models within the N_0 ranges for which these models work fine.

ACKNOWLEDGMENTS

We thank Martin Keane for his helpful recommendations in writing this paper. A.S. is grateful for financial support granted by the Gottlieb Daimler- und Karl Benz-Stiftung. This work was supported by CICYT (Spain), Project MAT97-1024.

[1] *Kinetics of Aggregation and Gelation*, edited by F. Family and D. P. Landau (North-Holland, Amsterdam, 1984).
[2] D. H. Sutherland, J. Colloid Interface Sci. **25**, 373 (1967).
[3] G. K. von Schulthess and G. B. Benedek, Macromolecules **13**, 939 (1980).
[4] J. E. Martin, J. P. Wicoxon, D. Schaefer, and J. Odinek, Phys. Rev. A **41**, 4379 (1990).
[5] G. Bole, C. Cametti, P. Codastefano, and P. Tartaglia, Phys. Rev. A **35**, 837 (1987).
[6] H. Y. Lin, H. M. Lindsay, D. A. Weitz, R. C. Ball, R. Klein, and P. Meakin, Phys. Rev. A **41**, 2005 (1990).
[7] D. Asnaghi, M. Carpineti, M. Giglio, and M. Sozzi, Phys. Rev. A **45**, 1018 (1992).
[8] M. L. Broide and R. J. Cohen, Phys. Rev. Lett. **64**, 2026 (1990).
[9] M. Carpineti and M. Giglio, Adv. Colloid Interface Sci. **46**, 73 (1993).
[10] J. Stankiewicz, M. Cabrerizo-Vilchez, and R. Hidalgo-Álvarez, Phys. Rev. E **47**, 2663 (1993).
[11] M. Von Smoluchowski, Z. Phys. Chem. **92**, 129 (1917).
[12] T. Vicsek, *Fractal Growth Phenomena* (Word Scientific, Singapore, 1992).
[13] B. B. Mandelbrot, *The Fractal Geometry of Nature* (Freeman, San Francisco, 1982).
[14] E. G. M. Pelssers, M. C. A. Stuart, and G. J. Fleer, J. Colloid Interface Sci. **137**, 350 (1990).
[15] E. G. M. Pelssers, M. C. A. Stuart, and G. J. Fleer, J. Colloid Interface Sci. **137**, 362 (1990).
[16] M. S. Bowen, M. L. Broide, and R. J. Cohen, J. Colloid Interface Sci. **105**, 605 (1985).
[17] M. S. Bowen, M. L. Broide, and R. J. Cohen, J. Colloid Interface Sci. **105**, 617 (1985).
[18] P. G. Cummins, E. J. Staples, L. G. Thompson, A. L. Smith, and L. Pope, J. Colloid Interface Sci. **92**, 189 (1983).
[19] N. Buske, H. Gedan, H. Lichtenfeld, W. Katz, and H. Sonntag, Colloid Polym. Sci. **258**, 1303 (1980).
[20] A. Elaissari and E. Pefferkorn, J. Chem. Phys. **95**, 2919 (1991).
[21] S. Stoll, V. Lanet, and E. Pefferkorn, J. Colloid Interface Sci. **157**, 302 (1993).
[22] R. Pecora, *Dynamic Light Scattering* (Plenum, New York, 1985).
[23] D. E. Guinnup and J. S. Schultz, J. Phys. Chem. **90**, 3282 (1986).
[24] T. M. Herrington and B. R. Midmore, J. Chem. Soc. Faraday Trans. **85**, 3529 (1989).
[25] M. Kerker, *The Scattering of Light and Other Electromagnetic Radiations* (Academic, New York, 1969).
[26] R. M. Ziff, in *Kinetics of Aggregation and Gelation* (Ref. [1]), pp. 191–199.
[27] B. V. Derjaguin and L. Landau, Acta Physicochim. URSS **14**, 63 (1941).
[28] E. J. Verwey and J. Th. G. Overbeck, *Theory of the Stability of Lyophobic Colloids* (Elsevier, Amsterdam, 1934).
[29] N. Fuchs, Z. Phys. **89**, 736 (1934).
[30] R. J. Hunter, *Foundations of Colloid Science* (Oxford University Press, New York, 1987), Vol. I, Chap. 7.
[31] H. Ohshima and T. Kondo, J. Colloid Interface Sci. **122**, 2 (1988).
[32] L. A. Spielman, J. Colloid Interface Sci. **33**, 562 (1970).
[33] K. Higashitani, T. Tanaka, and Y. Matsuno, J. Colloid Interface Sci. **63**, 551 (1978).
[34] A. Fernández-Barbero, Ph.D. thesis, Universidad de Granada 1994 (unpublished).
[35] A. Fernández-Barbero, A. Schmitt, M. Cabrerizo-Vilchez, and R. Martínez-García, Physica A **53**, 230 (1996).
[36] A. Fernández-Barbero,M. Cabrerizo-Vílchez, R. Martínez-García, and R. Hidalgo-Álvarez, Phys. Rev. E **53**, 4981 (1996).
[37] P. N. Pusey, D. E. Koppel, D. W. Schaefer, R. Camerini-Otero, and S. H. Koening, Biochemistry **13**, 952 (1974).
[38] A. Lips, C. Smart, and E. Willis, J. Chem. Soc. Faraday Trans. **67**, 2979 (1971).
[39] I. G. Clague and E. Dickinson, J. Chem. Soc. Faraday Trans. **80**, 1485 (1984).
[40] B. Berne and R. Pecora, *Dynamic Light Scattering* (Krieger, Malabar, FL, 1990).
[41] W. Hatton, P. McFadyen, and A. L. Smith, J. Chem. Soc. Faraday Trans. **70**, 665 (1974).
[42] J. Cahill, P. G. Cummins, E. J. Staples, and L. G. Thompson, J. Colloid Interface Sci. **117**, 406 (1987).
[43] L. Goren, J. Colloid Interface Sci. **36**, 94 (1971).
[44] J. Cahill, P. G. Cummins, E. J. Staples, and L. G. Thompson, Colloids Surf. **18**, 189 (1989).
[45] H. Gedan, H. Lichtenfeld, H. Sonntag, and H. J. Krug, Colloids Surf. **11**, 199 (1984).
[46] W. I. Higuchi, R. Okada, G. A. Sterter, and A. P. Lenberger, J. Pharm. Sci. **52**, 49 (1963).
[47] B. A. Mathews and C. T. Rhodes, J. Pharm. Sci. **57**, 557 (1969).
[48] A. Lips and E. J. Willis, J. Chem. Soc. Faraday Trans. **69**, 1226 (1973).
[49] J. W. Lichtenfelt, C. Pathmanoharan, and P. H. Wiersema, J. Colloid Interface Sci. **49**, 281 (1974).
[50] M. L. Broide and R. J. Cohen, J. Colloid Interface Sci. **105**, 605 (1985).
[51] M. L. Broide and R. J. Cohen, J. Colloid Interface Sci. **105**, 617 (1985).
[52] K. Higashitani, M. Kondo, and A. Matacle, J. Colloid Interface Sci. **142**, 204 (1991).
[53] B. V. Derjaguin and N. M. Kudryavetseva, Colloid J. **26**, 49 (1964).
[54] H. Gedan, H. Lichtenfeld, and H. Sonntag, Colloid Polym. Sci. **260**, 1151 (1982).
[55] M. S. Bowen, M. L. Broide, and R. J. Cohen, in Kinetics of Aggregation and Gelation (Ref. [1]), pp. 185–190.
[56] D. E. Koppel, J. Chem. Phys. **57**, 4814 (1972).
[57] J. C. Brown and P. N. Pusey, J. Chem. Phys. **62**, 1136 (1975).
[58] P. Meakin, T. Vicsek, and F. Family, Phys. Rev. B **31**, 564 (1985).
[59] P. G. J. Van Dongen and M. H. Ernst, Phys. Rev. Lett. **54**, 1396 (1985); J. Stat. Phys. **50**, 295 (1988).